Determining the off-target activity of antibiotics and novel translation initiation sites in mitochondria

James Marks[1,#,*] , Emma Young[1,**], Markus Hafner[1,#]

[1]RNA Molecular Biology Laboratory, National Institute for Arthritis and Musculoskeletal and Skin Diseases, NIH, Bethesda, MD 20892

Current address:
*Department of Biochemistry, Vanderbilt University School of Medicine, Nashville, TN 37237
**Department of Biological Anthropology, University of California, Los Angeles, CA 90095

[#]Corresponding authors: james.marks@vanderbilt.edu, markus.hafner@nih.gov

Abstract

The 13 mtDNA-encoded proteins are synthesized using a dedicated translation system that is more similar to bacterial systems than the cytoplasmic system. Consequently, many bacterial protein synthesis inhibitors, used as antibiotics, exhibit mitochondrial toxicity as off-target effects. However, whether these antibiotics act through the same mechanisms in mitochondria as in bacteria remains unclear. To address this, we characterized the impact of a panel of bacterial translation initiation and elongation inhibitors on mitochondrial translation through mitoribosome profiling. We found that the mechanism of action for every antibiotic, except telithromycin, is the same in both bacteria and mitochondria. Additionally, mitoribosome profiling data showed that *MT-ND1* and *MT-ND5* have incorrectly annotated translation initiation sites and suggested the presence of several translation initiation sites on ncRNAs that produce mitoribosome footprints, as indicated by the detection of mitoribosome footprints at these locations. This work demonstrates how antibiotics can inhibit mitochondrial translation by mechanisms identically or very similar to those found in bacteria and the utility of mitoribosome profiling for annotating mitochondrial genes.

Introduction

Mitochondria contain their own genome, which canonically encodes thirteen proteins. These proteins are essential building blocks of complexes I, III, and IV of the electron transport chain, as well as ATP synthetase. They are synthesized at the mitochondrial matrix by a dedicated translation system that is conserved from the ancestral bacteria that evolved into the present-day organelles through an endosymbiotic event[1]. As a result, mitochondrial translation is wholly distinct from cytoplasmic translation and utilizes its own mitochondrial ribosomes (mitoribosomes), tRNAs, and translation factors. The RNA components of the machinery are mitochondrially encoded, while its protein components are encoded in the nucleus, translated by the cytoplasmic ribosome, and subsequently imported into the mitochondria[2].

Chronic impairment of mitochondrial translation, most commonly through mutations in translation factors, results in disrupted mitochondrial function and causes diseases such as MERRF (Myoclonic Epilepsy with Ragged-Red Fibers)[3], MELAS (Mitochondrial Encephalopathy, Lactic Acidosis, and Stroke-like episodes)[4], and maternally inherited deafness[5,6]. Furthermore, acute inhibition of mitochondrial translation caused by the off-target action of antibiotics targeting the bacterial ribosome can also cause mitochondrial toxicity[7-11]. This toxicity can manifest as lactic acidosis, ototoxicity[12], nephrotoxicity[13], and peripheral neuropathy[14], depending on the specific antibiotic and the genetic background of the recipient[15]. While the United States has worked to regulate antibiotics with severe side effects, they remain a global issue. For example, chloramphenicol, whose use is discontinued in the United States, causes fatal aplastic anemia at a rate of 1 in 60,000[7] but remains widely prescribed in low-income countries due to its low production cost[16,17]. Surveys suggest that approximately 14.3 doses of antibiotics are administered per 1,000 people every day worldwide[18]. The toxic effects of antibiotics can be exacerbated when taken without medical supervision. In addition, safety concerns surrounding drugs like chloramphenicol and telithromycin, which are linked to liver failure[19], limit our pool of available antibiotics in the face of a rise in multidrug-resistant bacteria. Studying the off-target effects of these drugs can guide the development of safer therapies.

Multiple classes of antibiotics inhibit bacterial translation by binding functionally important sites on the ribosome and disrupting a specific process in translation, resulting in arrested translation on mRNAs at sites characteristic of the mechanism of inhibition[20,21]. In some instances, this relationship is straightforward. For example, the pleuromutilin antibiotic retapamulin binds to the peptidyl-transferase center (PTC) of the bacterial ribosome and impedes translation initiation

72 by interfering with the positioning of initiator tRNA[22], resulting in bacterial ribosomes accumulating
73 at start codons[23]. Inhibition by other antibiotics is more complicated, only disrupting translation
74 when specific sequences are being translated, called context-dependent translation arrest. This
75 is exemplified by chloramphenicol, which simultaneously interacts with the nascent peptide and
76 the peptidyl-transferase center at its binding site and disrupts accommodation of aminoacyl-tRNA,
77 thereby acting as an elongation inhibitor[24]. Due to chloramphenicol's interaction with the nascent
78 peptide, it selectively causes ribosomes to arrest translation when an alanine, serine, or threonine
79 is in the –1 (penultimate) position of the nascent peptide[25]. Additionally, chloramphenicol does not
80 interfere with the accommodation of glycine due to its minimal size. The mechanisms of these
81 and other antibiotics in bacteria have been determined by ribosome profiling and structural
82 studies. As well, structural studies have demonstrated the binding characteristics of antibiotics on
83 the mitochondrial ribosome[11,26,27]. However, it remains unclear whether chloramphenicol or other
84 antibiotics inhibit mitochondrial translation by identical mechanisms.
85 To determine the sites of translation arrest, we utilized mitoribosome profiling in HEK293
86 cells treated with a diverse panel of antibiotics[19,28,29]. Ribosome profiling allows for the mapping
87 of translating ribosomes with codon-level accuracy by identifying mRNA sequences occupied by
88 translating ribosomes. To do this, RNase treatment degrades mRNA unprotected by the ribosome
89 to generate ribosome-protected fragments (RPFs). Because cytoplasmic ribosomes significantly
90 outnumber mitoribosomes, mitoribosomes containing the mitochondrial RPFs (MRPFs) are
91 isolated through sucrose gradient fractionation, where the cytoplasmic ribosome and
92 mitoribosome sediment in the 80S and 55S fractions, respectively (Figure 1A). RPFs are isolated
93 and quantified by next-generation sequencing. Increases in MRPFs reveal the specific codons
94 and sequence contexts prevalent at sites at which mitochondrial translation arrests due to
95 antibiotic treatment.
96 Understanding the mechanisms of translation inhibitors in mitochondria can guide the
97 development of therapeutics that are more selective to the bacterial ribosome and lay the
98 groundwork for determining how these therapeutics disrupt mitochondrial function. In this study,
99 we utilized mitoribosome profiling in the presence of the bacterial protein synthesis inhibitors
100 retapamulin, tiamulin, josamycin, erythromycin, chloramphenicol, and linezolid to determine their
101 mechanism of action. We found that the mechanism of mitochondrial inhibition is the same as
102 bacterial inhibition for all inhibitors except telithromycin. While telithromycin selectively arrests
103 bacterial ribosomes when either arginine (R) or lysine (K) is in the -1 position of the nascent chain
104 and A-site, called an R/K-X-R/K motif[30], it instead arrests mitochondrial translation at an R/K/A-

105 X-K motif, suggesting an underlying difference in the mechanism of the two systems. Additionally,
106 nucleotide-level precision of mitoribosome profiling also allowed us to precisely annotate the
107 mitochondrial gene structure. We found that *MT-ND1* and *MT-ND5* genes use alternative
108 translation initiation sites and identified a putative open reading frame on the *MT-RNR1* gene.
109 This work demonstrates that mitoribosome profiling is an effective tool to study the fundamentals
110 of mitochondrial translation and the mechanisms of translation impairment affecting human
111 health.

112

Results

RNase I generates highly phased mitoribosome footprints

To optimize the mitoribosome profiling method, we tested two different RNases typically used for ribosome footprinting, RNase I and MNase, followed by the isolation of the 55S mitoribosome by sucrose gradient fractionation. We mapped the sequence reads to the mitochondrial genome and its thirteen open reading frames (ORFs). For each mapped sequence read, we inferred the position of the ribosomal P-site using a 13-nucleotide (nt) offset from the 5' end, determined by the analysis of footprint distribution surrounding the initiation sites of *MT-ND4*, *MT-ND6*, and the newly reported *MT-ND5-dORF*. We observed coverage across mitochondrial ORFs, suggesting we captured translating mitoribosomes (Figure 1B). Furthermore, analysis of MRPF lengths revealed a distinct difference between the RNase I and MNase-digested footprint. While both libraries are enriched for reads ~30 nt in length, MNase footprints showed a bimodal distribution, with a clear secondary peak at ~22 nts (Figure 1C), which may indicate that MNase-treatment may have captured two distinct conformations of the ribosome. To determine the quality of the ribosome profiling data, we calculated read phasing, which occurs when a nuclease creates uniform MRPFs and the resulting ends of the MRPFs reflect the 3-nt periodicity of elongating ribosomes. While both datasets do show clear phasing, the read phasing is more biased toward position 1 of the codon in the RNase I-treated sample, indicating slightly more consistent digestion (Figure 1D, Table S1). Nevertheless, we observed similar levels of footprint abundance per gene, with the only notable exceptions being that RNase I-digested footprints were enriched on *MT-ND3* and depleted on *MT-ND4L* and *MT-ND6* (Figure 1E). While the cause of the difference is unclear, we did not expect it to interfere when comparing an antibiotic-treated sample to a control. Read coverage also appeared similar across the two methods, with 85%-87% codons having between 2 and 50 reads mapping to them (Figure 1F). Overall, these results indicated that both MNase and RNase I digestion capture mitoribosome footprints with only minor differences. Considering the improved read phasing, we selected RNase I for our subsequent mitoribosome profiling experiments.

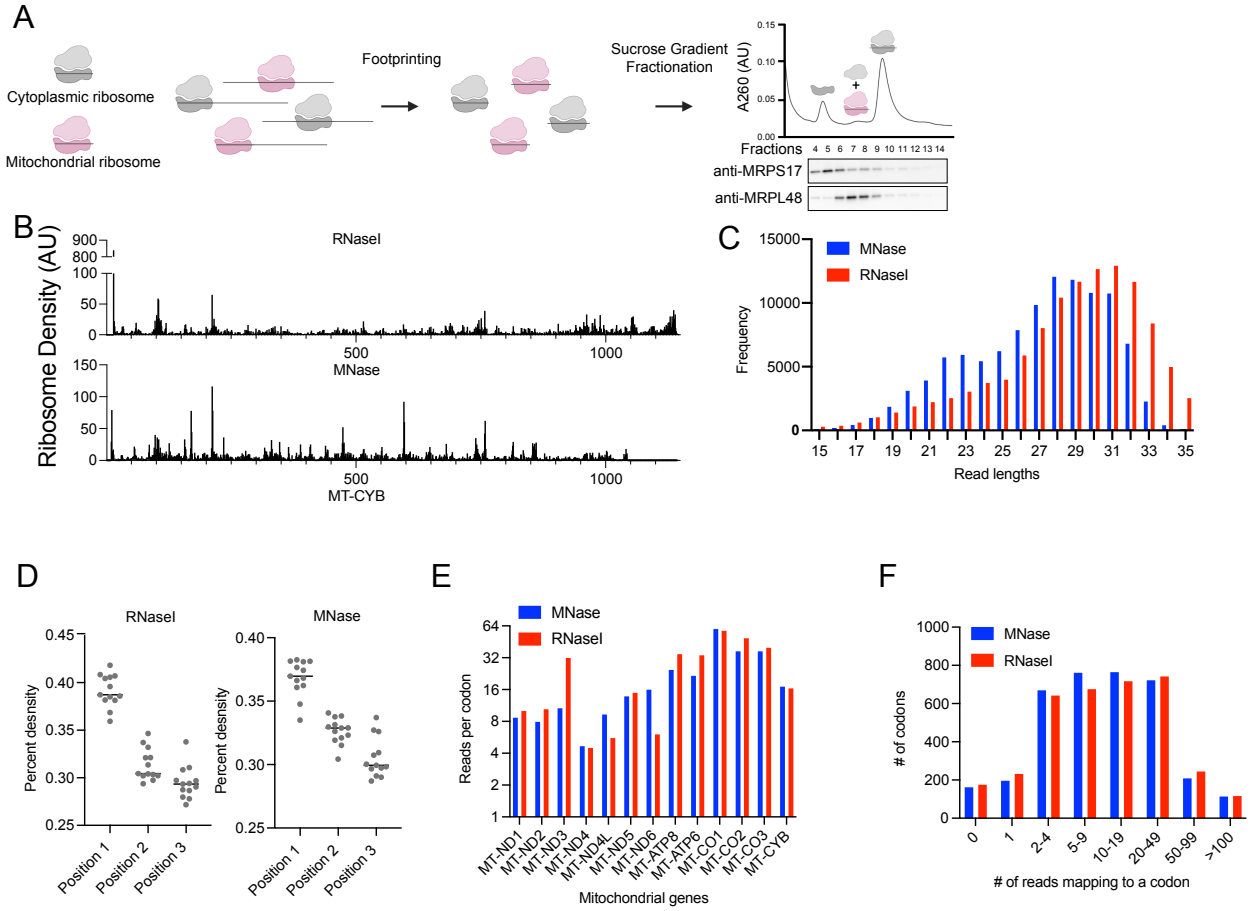

Figure 1. Mitoribosome profiling captures elongating ribosomes.

(A) Schematic representation of mitoribosome footprinting and separation from cytoplasmic ribosomes by differential centrifugation. (B) Coverage of MRPFs on *MT-CYB* from mitoribosome profiling generated by either RNase I or MNase footprinting. (C) Distribution of read lengths of MRPFs mapping to the mitochondrial genome. (D) Read phasing analysis of MRPFs, where the 5' ends of reads are grouped by their subcodon position. Each dot represents an individual mitochondrial gene. (E) Average coverage of mitochondrial genes, calculated by dividing the total number of reads mapping to an ORF and dividing by the length of the ORF. (F) Distribution of mitochondrial codons grouped by the number of mitoribosome P-sites assigned to them.

154 **Retapamulin, tiamulin, and josamycin inhibit translation initiation**

155 First, we examined the impact of three antibiotics – retapamulin, josamycin, and tiamulin – on
156 translation initiation or mitochondrial translation. Retapamulin and tiamulin are members of the
157 pleuromutilin class of antibiotics. They work by binding to the peptidyl transferase center (PTC)
158 of the bacterial ribosome and disrupting initiator tRNA and A site tRNA positioning (Figure 2A,
159 left)[22,23,31-33]. Josamycin is a macrolide antibiotic that binds in the nascent peptide exit tunnel near
160 the PTC and arrests bacterial ribosomes at initiation by interfering with A-site tRNA positioning
161 (Figure 2A, right)[34]. We sought to understand whether these antibiotics also target translation
162 initiation in mitochondria. To this end, we treated HEK293 cells with high concentrations of these
163 antibiotics (100 µg/ml of tiamulin and josamycin, 10 µg/mL of retapamulin) for 30 minutes,
164 performed mitoribosome profiling, and compared the treated experiments to a DMSO-treated
165 control.

166 We mapped MRPFs to the 13 mitochondrial genes. On *MT-CYB* and all other genes, we
167 observed that after treatment with antibiotics, reads accumulated at the 5' end of the transcript
168 and MRPFs across the rest of the coding region were lost or decreased (Figures 2B, S1). We
169 quantified the percentage of MRPFs mapping at the 5' end relative to the total ORF, excluding
170 polycistronic mRNAs. Treatment with translation initiation inhibitors increased the percentage of
171 those reads from 2.4 to 5.2-fold relative to the DMSO-treated cells (Figure 2C). Additionally, we
172 quantified the cumulative footprint abundance moving from the start to the stop codon (Figure
173 2D). While ribosome footprints are generally evenly spread across the open reading frame in the
174 DMSO control, MRPFs from cells treated with the initiation inhibitors showed a sharp increase in
175 the percentage of reads found at the 5' end. Together, these results indicate that retapamulin,
176 tiamulin, and josamycin inhibit mitochondrial translation initiation, likely by the same mechanism
177 as in prokaryotes.

178

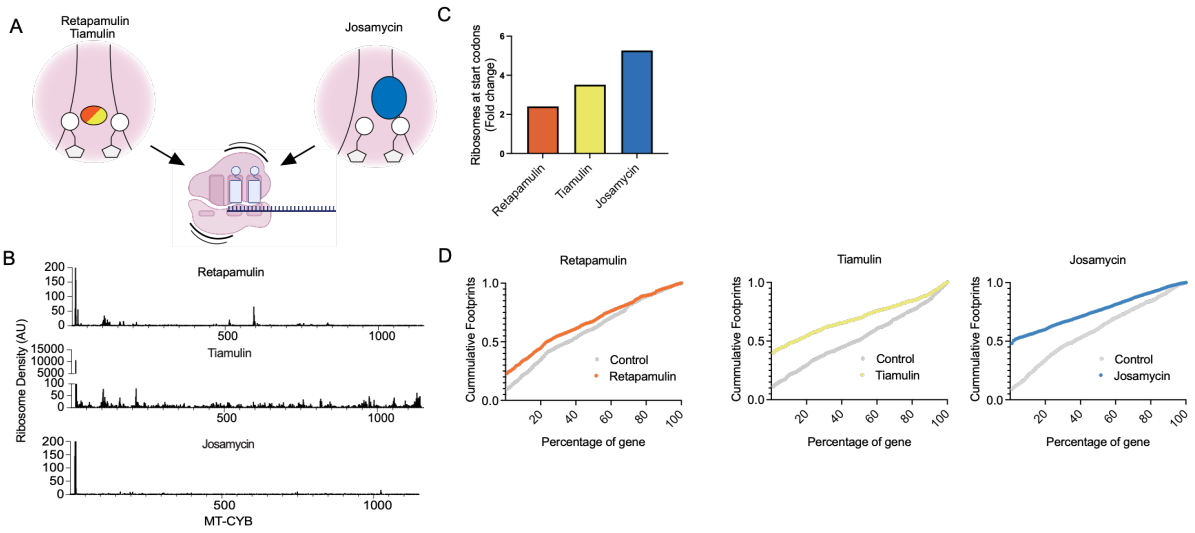

Figure 2. Inhibition of translation initiation in mitochondria.

(A) (Left) Schematic representation of retapamulin (orange) or tiamulin (yellow) binding to the PTC and disrupting the first round of elongation. (Right) Josamycin (blue) disrupts accommodation of the first aminoacyl-tRNA. All three inhibit initiation in bacteria. (B) MRPF coverage of *MT-CYB* treated with either retapamulin, tiamulin (note y-axis is segmented), or josamycin. (C) Average fold change increase in the percentage of reads that map to the 5' of mitochondrial transcripts. (D) Cumulative distribution of ribosome density normalized across all mitochondrial ORFs.

190 **Chloramphenicol, linezolid, and telithromycin arrest mitochondrial translation in a context-**
191 **dependent manner**
192 Chloramphenicol, linezolid, and telithromycin selectively inhibit bacterial translation when
193 ribosomes are translating specific sequences, in a process called context-dependent translation
194 arrest[25,30]. Linezolid, like chloramphenicol, induces context-dependent arrest when alanine,
195 serine, or threonine is at the penultimate position of the nascent peptide (Figure 3A, left). Unlike
196 chloramphenicol and linezolid, telithromycin binds in the nascent peptide exit tunnel near the PTC
197 and adjacent to the nascent peptide[35]. During elongation, telithromycin causes ribosomes to
198 arrest translation at an R/K-X-R/K motif, when the identity of both the penultimate position of the
199 nascent peptide and the incoming aminoacyl-moiety is either arginine or lysine (Figure 3A, right).
200 We carried out mitoribosome profiling on HEK293 cells treated with either antibiotic to
201 understand whether these context-dependent translation inhibitors arrest mitoribosomes in the
202 same manner as they arrest bacterial ribosomes. Unlike the cells treated with initiation inhibitors,
203 cells treated with chloramphenicol or linezolid carried ribosome density throughout the entirety of
204 the ORF, suggesting that, as expected, they were not acting as inhibitors of initiation (Figures 3B,
205 S1). Cells treated with telithromycin did show a slight increase in MRPFs abundance at the 5' end
206 of *MT-CYB.* However, across all genes, the levels of MRPFs at the 5' end were not near the levels
207 seen when using the initiation inhibitor retapamulin and were more similar to chloramphenicol,
208 linezolid, and the DMSO control (Figure 3C). The cumulative distribution of MRPFs suggested
209 that ribosome density was biased towards the 5' end of the gene for chloramphenicol and
210 telithromycin, but not significantly for linezolid (Figure 3D). These results suggest that these three
211 antibiotics are not acting as initiation inhibitors and that linezolid and telithromycin redistribute
212 MRPFs to the 5' end of the ORF.
213 Next, we determined whether this observed redistribution of elongating ribosomes was
214 dependent on the context of the sequence being translated. We calculated the average change
215 of MRPFs depending on the identity of the amino acid at either the -1, P-site, or A-site positions.
216 For both chloramphenicol and linezolid, we observed a specific increase in ribosome footprints
217 when mitoribosomes encountered codons for alanine, serine, or threonine in the -1 position, with
218 a 2-, 2.2-, and 1.3-fold change for chloramphenicol and a 2.3-, 1.4-, and 1.6-fold change for
219 linezolid, respectively (Figure 3E). Additionally, we also observed context-dependent translation
220 arrest induced by telithromycin. Unlike the R/K-X-R/K motif observed in bacteria, we found that
221 telithromycin caused mitoribosomes to arrest at sites with a lysine positioned in the A-site, with
222 an average 2.5-fold increase in MRPFs around those sites, and that neither residue was enriched

223 in the -1 position. Due to the limited size of the mitochondrial genome, there are only nine
224 instances of the R/K-X-R/K motif; nevertheless, when we observed the positions with the greatest
225 fold change, 3 of the top 4 contained the motif with lysine in the A-site (Figure 3F), suggesting
226 that the motif was at least partially recapitulated. To specifically look for the motif, we calculated
227 the average fold change when we fixed arginine or lysine in the A-site and varied the identity of
228 the -1 amino acid (Figure 3G). We found that when lysine was in the A-site while either arginine,
229 lysine, or alanine was in the -1 position, there was strong arrest (> 5-fold change). However, when
230 arginine was in the A-site, we did not observe a strong stalling event with any -1 position residue.
231 Therefore, in mitochondria, telithromycin induces stalling at R/K/A-X-K motifs. This motif appears
232 in only 6 of the 13 mitochondrially encoded genes, indicating that mitochondrial protein synthesis
233 is unequally inhibited (Figure S2A, B). We concluded that the mechanism underlying context-
234 dependent translation arrest for telithromycin is different in mitochondria compared to bacteria.
235

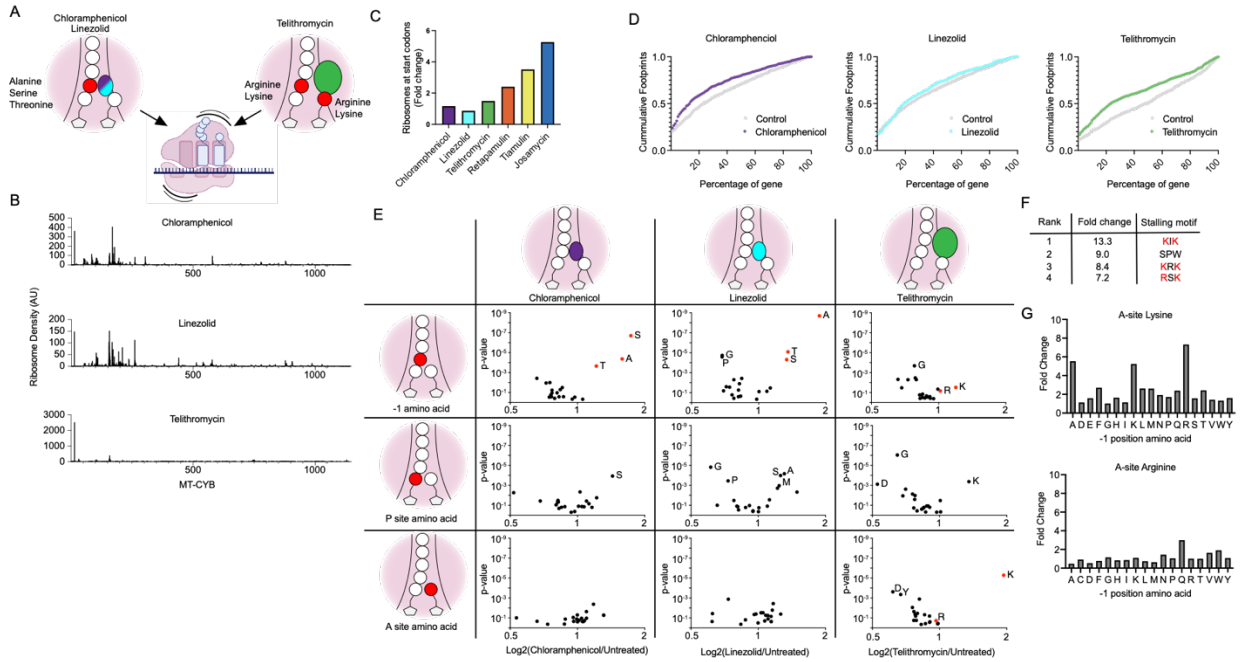

Figure 3. Context-dependent translation arrest by elongation inhibitors.

(A) Schematic representation of chloramphenicol (purple), linezolid (cyan), and telithromycin (green) inducing context-dependent translation arrest. (B) MRPF coverage of *MT-CYB* from cells treated with either chloramphenicol, linezolid, or telithromycin. (C) Average fold change increase in the percentage of reads that map to the 5' of mitochondrial transcripts. (D) Cumulative distribution of ribosome density normalized across all mitochondrial ORFs. (E) Volcano plots of changes in MRPF fold change from cells treated with translation inhibitors. Each dot is the mean $\log_2$-fold change grouped by the identity of the -1 amino acid (top), P-site amino acid (middle), or A-site amino acid (right). (F) The top 4 strongest stalling sites induced by telithromycin treatment. Red amino acids indicate a classical R/K-X-R/K stalling motif. (G) Fold change in ribosome density, calculated as $2^{\text{mean}(\log2(\text{Telithromycin/Control}))}$. Bars differ in the identity of the P-site amino acid and contain either a lysine in the A-site (top) or arginine (bottom).

251 **Translation initiation on *MT-ND1 and MT-ND5* occurs at an alternative start codon**
252 During the process of assigning the P-site positions of MRPFs, we observed that no ribosomes
253 were assigned in the first 13 nucleotides of the 5' end of the transcript. This is not surprising,
254 considering that mitochondrial transcripts often have no or very short 5' untranslated regions -
255 typically less than 4 nts long - and we applied a 13-nt offset from the 5' end of MRPFs. It reasons
256 that as mitoribosomes begin translation on a leaderless mRNA, the 5' end of the resulting MRPF
257 would have a full-length region 3' of the P-site and no sequence 5' of the P-site. As a ribosome
258 moves down the transcript, the 5' end of the MRPF would increase until it is accessible for
259 digestion, at which point it would generate 31 nt-long MRPFs (Figure 4A). As accurate mapping
260 of mitoribosomes at initiation could be a useful tool to understand mitochondrial translation, we
261 attempted to map the location of initiating mitoribosomes at the 5' end using footprint length, rather
262 than the 5' offset. Because mitoribosome profiling with MNase generated a population of
263 ribosomes with short MRPFs, we hypothesized that these footprints could be indicative of
264 capturing initiating ribosomes (Figure 1C). We plotted the distribution of MRPFs from 20 to 34 nts
265 in length that mapped to the 5' end of the 11 leaderless or short leader ORFs and compared them
266 to reads mapping to the whole ORF. We observed that MRPFs 22-23 nts in length were 6-fold
267 more abundant and MRPFs >28 nts in length were depleted compared to the whole ORF (Figure
268 4B). As mitochondrial ORFs vary in the length of their 5' UTR and we expect most ribosomes to
269 be positioned at the start codon, we tested whether leaderless ORFs were enriched in shorter
270 reads compared to ORFs preceded by a short leader. Leaderless ORFs, such as *MT-CO2*, *MT-*
271 *CO3*, and *MT-ND4L,* contained MRPFs mainly 20-23 nucleotides in length at the 5' end (Figure
272 4C, top). *MT-ATP8*, which contains a start codon beginning at the third nt, contained footprints
273 that were 22-24 nt long, and *MT-CO1,* with a start codon at the fourth nt, contained MRPFs 23-
274 24 nt long (Figure 4C, middle). Not only did we observe longer MRPFs in short leader ORFs, but
275 the size of the MRPFs also appeared proportional to the location of the start codon. Together,
276 these results indicate that the size of the footprint is directly related to the start codon position at
277 the 5' end of mitochondrial mRNAs.
278 Two genes, *MT-ND*1 and *MT-ND5,* deviated from this trend. The annotated start site for
279 *MT-ND5* is a leaderless AUA codon (a start codon in mitochondria), but we observed few 20-22
280 nt MRPFs (Figure 4C, bottom). Similarly, the annotated start site for *MT-ND1* is also an AUA
281 codon that begins at the third nt, and it is depleted in reads for MRPFs that are smaller than 25
282 nts. Instead, MRPFs derived from the 5' end of both genes are enriched in longer reads: 27 nts-
283 long for *MT-ND5* and 28-29 nts-long for *MT-ND1*. Curiously, the third codon for both genes is an

284 in-frame AUG, and the read lengths proportionally correspond to mitoribosomes positioned at
285 these codons, suggesting mitoribosomes initiate translation at these sites. MRPFs generated from
286 cells treated with initiation inhibitors and footprinted by MNase yield similarly sized reads at the 5'
287 end of *MT-ND1* and *MT-ND5* (Figure S3). Using protein mass spectrometry, we tested whether
288 peptides matching the N-terminus of these proteins would correspond to initiation at the canonical
289 start codons or alternative start codons. We identified a peptide that mapped to the N-terminal
290 region of MT-ND1 but lacked the first two amino acids, accordant with translation initiating from
291 the alternative start codon (Figure 4D). While we did not identify N-terminal peptides mapping to
292 MT-ND5 from our mass spectrometry data, the protein mass spectrometry database MassIVE[34]
293 covered the N-terminal region of MT-ND5 (Figure 4E). Consistent with our mitoribosome profiling
294 data, the majority of N-terminal fragments did not include the amino acids from the annotated start
295 or second codon but began with methionine at codon 3. We also observed that MRPFs on *MT-*
296 *ND6,* which initiates at the first of two AUG codons immediately at the 5' end, correlated to
297 ribosomes positioned at both AUG codons, indicating that this gene may initiate translation from
298 the second AUG codon as well. However, we did not observe any peptides mapping to the N-
299 terminus of *MT-ND6*. Together, these data show that *MT-ND1* and *MT-ND5* may not initiate from
300 their canonical AUA codons but may use alternative in-frame AUG codons. Additionally, our
301 findings indicate that the mapping of mitochondrial translation initiation events by size, rather than
302 5' offset, is an accurate strategy when used in conjunction with MNase footprinting.
303

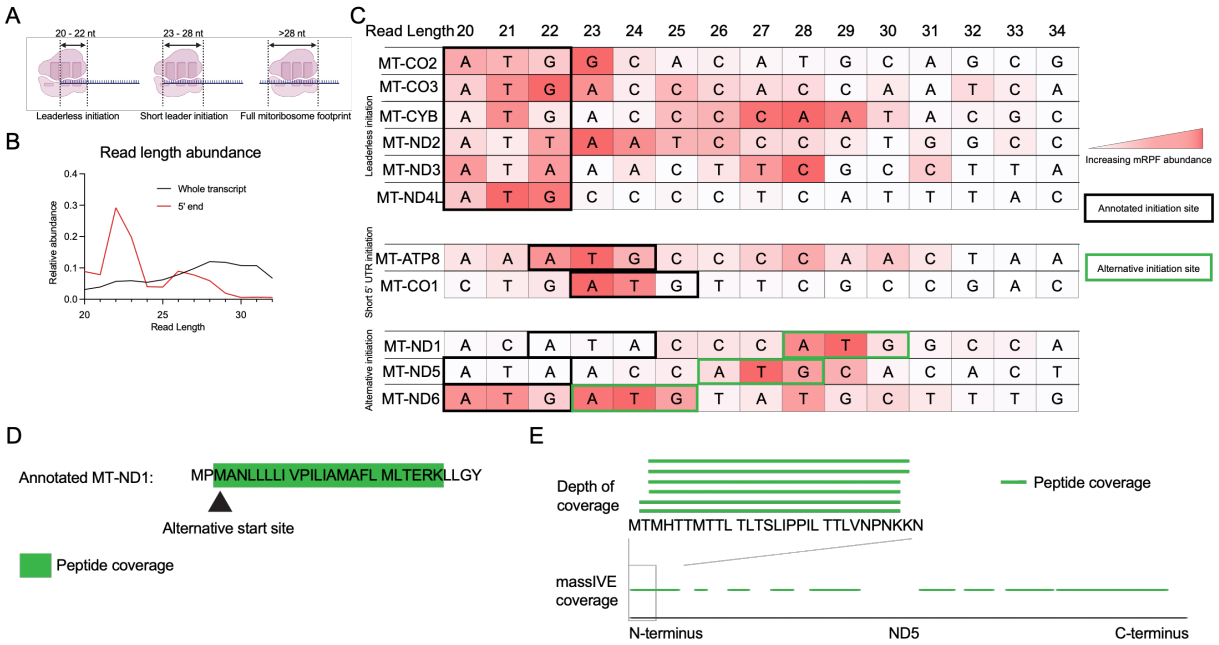

Figure 4. MRPF sizes indicate use of alternative initiation sites.

(A) Schematic representation of changing MRPF sizes as a function of the mitoribosome's position near the 3' end of mRNAs. (B) Read length measurement of reads mapping to the 5' ends of mitochondrial transcripts (red) compared to the entire ORF (black). (C) Read lengths of MRPFs mapping to the 5' ends of mitochondrial transcripts. Each row contains the nucleotide sequence of each transcript starting from the 5' end. The coloring of the box is proportional abundance of MRPFs with read lengths from 20-34 nts. Nucleotide sequence and read abundance are overlayed to compare the abundance of reads to potential ribosome start sites. Transcripts are grouped by being leaderless, having a leader, or having a potential alternative start site. Black boxes indicate annotated start codons and green boxes indicate alternative initiation sites. (D) Visual representation of the peptide coverage (green bars or highlights) from mass spectrometry data covering the N-terminus of *MT-ND1* or (E) *MT-ND5.*

318 **Mitoribosome profiling may reveal novel translation events**

319 During our analysis of 5' end mapping, we did not remove reads mapping to non-coding RNAs
320 (ncRNAs) before mapping to the mitochondrial genome and performing P-site assignment.
321 Consequently, we observed that some tRNAs and rRNAs had an abundance of reads mapping
322 to 13 nts away from their 5' ends, similarly to what we observe on mRNAs for translation initiation.
323 In addition, some of these ncRNAs contained a potential start codon near the 5' end. These reads
324 could either be products of random digestion of the abundant background of ncRNAs or be
325 genuine MRPFs. We hypothesized that if these reads were the result of mitoribosomes initiating
326 or attempting to initiate translation at the 5' end of the ncRNAs, then we could use the same
327 analysis of read length distribution at 5' ends of mRNAs we performed above and determine of
328 the sizes correlated to an AUG, AUU, GUG, or UUG as potential start codons. While GUG and
329 UUG are not used in canonical mitochondrial initiation, they were included in the search because
330 noncanonical initiation has been observed at GUG[36] , and both are frequently utilized in bacterial
331 initiation. We identified sites on four tRNAs that contained MRPFs with a size that correlated to
332 either AUG or UUG codons (Figure 5A). The predicted ORFs and thus resulting potential
333 translation events varied widely. On *MT-TF*, the start codon is followed by an immediate stop
334 codon. The ORF on *MT-TI* is three codons long and terminates with the non-canonical
335 mitochondrial termination codon AGA. On *MT-TY, a* 7-codon ORF is terminated by a UAA codon.
336 *MT-TS1* contains the largest open reading frame identified on tRNAs, at 20 codons, and it
337 terminates with the U AGA sequence, as used in *MT-CO1*[37]. Additionally, we identified a putative
338 start site at the 5' end of *MT-RNR1* (Figure 5A), and mitoribosome profiling of cells treated with
339 initiation inhibitors and digested with MNase shows similar footprint sizes (Figure S3). However,
340 this site did not occur at a canonical AUG or AUU codon, but instead at a UUG codon. This
341 putative start codon is followed by a 58-codon ORF and terminates at a UAG stop codon.

342 To determine whether translation elongation occurs at these putative ORFs, we
343 determined the read phasing characteristic for MRPFs derived from translating ribosomes at
344 these ORFs. However, the sites on *MT-TF*, *MT-TI*, and *MT-TY* are short and close to the 5' end,
345 hindering phasing analysis and thus do not allow us to conclude whether our sequence reads are
346 indicative of translation. While the ORF on *MT-TS1* is longer, MRPF density was low, and we did
347 not observe read phasing and thus it is likely not translated (not shown). The reads mapping to
348 the ORF on *MT-RNR1* had a phasing profile similar to those mapping to the 13 canonical
349 mitochondrial genes (Figure 5B). In contrast, reads mapping to the remainder of *MT-RNR1* or
350 mapping to the region of *MT*-RNR2 that codes for the putative mitochondrial micropeptide

351 Humanin show no or conflicting read phasing. When compared to the amino acid composition of
352 the mitochondrially-encoded proteome, the amino acid composition of the resulting peptide shows
353 a stronger positive correlation (R^2=0.534) (Figure 5C) to the remaining non-coding portion of *MT-*
354 *RNR1* (R^2=0.241) (Figure 5D). Although mitoribosome profiling suggests that this putative ORF
355 is translated, we did not detect any corresponding peptides in the protein mass spectrometry of
356 isolated mitochondria. Nevertheless, our mass spectrometry dataset, or the MASSIVE database,
357 does not cover many regions of the mitochondrial proteome, and thus, the absence of a spectrum
358 is not necessarily evidence that the peptide is not translated. The read phasing analysis suggests
359 this region of *MT-RNR1* is translated and could encode a 15th mitochondrial protein. Overall, this
360 data shows that our mitoribosome profiling can be used as a tool to study non-canonical
361 translation events resulting from ncRNAs.
362

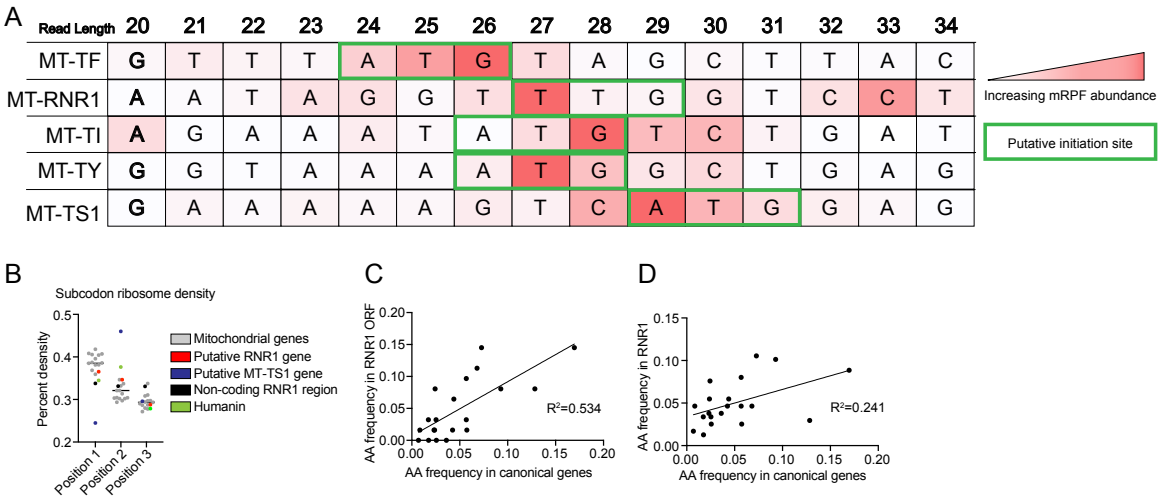

Figure 5. MRPFs on ncRNAs indicate potential novel ORFs

(A) Read lengths of MRPFs mapping to the 5' end of ncRNAs. Each row contains the nucleotide sequence beginning from the 5' end of listed ncRNAs. The coloring of the box is proportional the abundance of MRPFs with read lengths 20-34 nts. The nucleotide sequence and read MRPF abundance are overlayed to identify potential new start sites. Putative start sites are indicated by green boxes. (B) Read phasing analysis of all canonical ORFs (grey), a mutative ORF located on *MT-RNR1,* the non-coding region of *MT-RNR1,* and Humanin. (C) A correlation plot comparing the frequence of amino acid usage in canonical ORFs compared to the putative ORF on *MT-RNR1* or (D) the non-coding region of *MT-RNR1.*

375 # Discussion

376 In this work, we sought to understand the mechanisms of bacterial protein synthesis inhibitors on
377 their primary off-target, the mitoribosome. We found that inhibitors of bacterial translation
378 initiation, retapamulin, tiamulin, and josamycin, also act as initiation inhibitors in mitochondria.
379 Likewise, chloramphenicol and linezolid selectively inhibit elongation when the mitoribosome
380 carries either an alanine, serine, or threonine in the penultimate position of the nascent peptide,
381 matching their mechanism in bacteria. In contrast, the context-dependence of telithromycin
382 differed when arresting mitoribosomes, wherein it preferentially arrested translation at the R/K/A-
383 X-K motif.

384 Context-dependent translation arrest by chloramphenicol and linezolid suggests
385 similarities between the binding of the bacterial ribosome and the mitoribosome. Structural and
386 biochemical studies have demonstrated that binding of chloramphenicol and linezolid is stabilized
387 by alanine, serine, or threonine in the penultimate position of nascent peptide[38,39]. Our findings
388 suggest a similar or identical interaction is occurring in the mitoribosome. In contrast, these
389 inhibitors are unable to inhibit peptide bond formation in bacteria when glycine is positioned in the
390 A-site, due to the minimal size of the side chain, allowing the inhibitor and the aminoacyl-moiety
391 to coexist in the PTC. We did not observe a lack of mitoribosome translation arrest when glycine
392 was positioned in the A-site. This may have technical reasons, e.g., it may be caused by an
393 insufficient depth in sequencing or indicate that the relatively small mitochondrial genome limits
394 the variety of stalling and non-stalling events we can observe. But more likely it shows that
395 chloramphenicol and linezolid are capable of arresting translation when glycine is in the A-site.
396 Recently, mitoribosome profiling analysis showed that chloramphenicol added during lysis did not
397 induce context-dependent translation arrest[40]. This suggests that during lysis, there is insufficient
398 mitochondrial translation to induce a redistribution of mitoribosomes rather than an inability of the
399 chloramphenicol to induce context-dependent arrest.

400 During the preparation of this manuscript, two other groups studied the effect of translation
401 inhibitors on mitochondrial translation. One group's mitoribosome profiling in the presence of
402 chloramphenicol and linezolid agreed with our observed context-dependent translation arrest[41].
403 The structure of linezolid in the mitochondrial peptidyl-transferase center also suggested some
404 nuanced differences in binding between the bacterial and the mitochondrial ribosome. Another
405 group carried out mitoribosome profiling in the presence of retapamulin[40]. However, they
406 observed additional ribosome density throughout the coding region and potentially some
407 associated with putative start codons. This differs significantly from our observed accumulation at

408 only annotated start sites and may be due to differences in mitoribosome profiling methods.
409 Future work may reveal how each strategy contributes to our understanding of mitochondrial
410 translation.

411 Inhibition of mitochondrial translation through either small molecules or mutations
412 localized in mitochondrial translation factors can induce a wide range of pathologies[42-44]. However,
413 it is unclear how or whether the relationships between the mechanism of translation inhibition
414 relate to the resulting disease. Recently, the proteins mtRF-R and MTRES1 were shown to act
415 as quality control factors, rescuing stalled mitoribosomes by removing the nascent peptide and
416 peptidyl-tRNA[45]. In addition, treatment with antibiotics can reduce the presence of polyamines in
417 the mitoribosome, potentially reducing translation[46]. As the mitoribosome can arrest translation
418 through a variety of mechanisms and small molecules, it remains unclear whether these factors
419 can rescue all stalled mitoribosomes or decrease the translation rate to reduce the total amount
420 of translation arrest. Further work to dissect the relationship between mechanisms of inhibition,
421 activation of rescue factors, and stress response can complement our understanding of
422 pathologies resulting from mitoribosomopathies and antibiotic treatment.

423 In this study, we also reported that the translation start codon of two mitochondrial genes,
424 *MT-ND1* and *MT-ND5*, does not use the annotated AUA codon, but instead begins translation
425 from a nearby in-frame AUG codon. Others have noted that haplogroups L1b and F2 contain a
426 single nucleotide polymorphism at either position T3308C or T12338C, respectively, which
427 disrupts the annotated AUA start codons of *MT-ND1* and *MT-ND5* yet does not result in any
428 discernible pathogenicity[47-49]. The authors noted that the same AUG codons we identified as start
429 codons could be used in lieu of the canonical AUA start codons. Because we observe MRPF
430 lengths primarily correlating with the AUG codons, we suggest that these downstream start
431 codons are the primary start site for these genes, though this does not preclude the use of both
432 sites. Given the limited examples of translation initiation sites inherent to the mitochondrial
433 genome, the reannotation of 2 sites is a significant revision and can guide future work to
434 understand how start codon selection occurs in mitochondria.

435 Recently, mitoribosome profiling was used to identify an open reading frame in region
436 immediately 3' of the gene *MT-ND5,* which we confirmed observing in our profiling experiments[50].
437 However, this uses an internal initiation mechanism for polycistronic genes, similar to *MT-ND4*
438 and *MT-ATP6.* Until now, accurate mapping of mitochondrial translation events at the 5' ends of
439 transcripts has been unavailable. We identified MRPFs that map to putative start codons
440 occurring on mitochondrial MT-tRNAs and *MT-RNR1*, based on the size of the reads occurring at

441 the 5' end of the RNA and their relationship to a start codon localized in the sequence. The site
442 of *MT-RNR1* was further supported by analysis of the resulting ORF, suggesting translation
443 initiation and elongation occurs. Curiously, $tRNA^{Tyr}$, encoded by *MT-TY*, is polyadenylated during
444 processing, which may be related to our identification of a ribosome binding event on this tRNA[51].
445 Due to both the short ORFs, minimal read coverage, and lack of a detectable peptide we could
446 not determine if translation elongation occurred on the mitochondrial tRNAs. These sites may be
447 unproductive mitoribosome binding events or simply from tRNAs partially digesting during MNase
448 treatment. Future work is needed to understand whether these are actual translation events and
449 to determine the function of these potential novel peptides. Together, our findings improve our
450 understanding of mitochondrial translation initiation, gene expression, and the mechanisms of
451 translation inhibition.
452

453 # Materials and Methods

454 **Isolation of mitoribosomes for profiling and western blotting**

455 Mitoribosome profiling was carried out in HEK293 Flp-In T-REx cells. 15 cm plates were treated
456 with either DMSO as a control or 100 µg/mL of protein synthesis inhibitor for 1 hour, washed with
457 4°C PBS, and flash frozen by floating the plate on liquid nitrogen. Cells were collected by scraping
458 on ice with 600 µL of lysis buffer (1.5x Lysis buffer (30 mM Tris–HCl pH 7.8, 150 mM KCl,
459 15 mM $MgCl_2$, 1.5 mM DTT, 1.5% Triton X-100, 0.15% NP40, 1 × complete phosphatase
460 and protease inhibitors)) and lysed by passing through a 27-G needle 10 times. Lysate was
461 centrifuged for 10 minutes at 21,000 g at 4°C, and the supernatant was collected. 300 µL of lysate
462 was footprinted with either digested with 1,5000 U of MNase, 10 µL of SUPERase-In, and 5 mM
463 of $CaCl_2$ at 22°C for 1 hour and stopped by adding EGTA to a concentration of 6 mM or with 8
464 U/µL of RNase I at 22°C for 1 hour and stopped by adding 10 µL of SUPERase-In. Titration of the
465 digestion enzymes was not performed and is based on previous published work[29,50]. The digestion
466 was clarified by centrifugation at 21,000 g for 5 minutes. Lysates were loaded onto a 5%-30%
467 sucrose gradient (20 mM Tris-HCl, pH 7.8, 100 mM KCl, 10mM $MgCl_2$, 1 mM DTT) and spun for
468 2.5 hours at 40,000 rpm in a SW40 rotor. 55S mitoribosome fractions were collected using a
469 BioComp Fractionator and MRPFs were isolated by SDS/hot phenol/chloroform extraction.
470

471 **Mitoribosome profiling library construction**

472 Samples were run on a 15% TBE-Urea polyacrylamide gel and footprint sizes from 15-34 nts
473 were excised and footprints were eluted in 0.3 M NaOAc, 1 mM EDTA, and 0.25% SDS followed
474 by purification by Oligo Clean & Concentrator. Samples were treated with Quick CIP. 3' adapters
475 (5'-rAppNN-6 nt UMI-TGGAATTCTCGGGTGCCAAGG-L) were ligated using Rnl2(1-249)K227Q
476 ligase for 2 hours at 16°C and pooled. Pooled samples were treated with T4 PNK for 30 minutes
477 at 37°C. A 5' chimeric DNA-RNA adapter (GTTCAGAGTTCTACAGTCCGACGATCrNrNrNrN)
478 was ligated to the samples with T4 RNL1. Reverse transcription was carried out using SuperScript
479 IV followed by PCR amplification by Taq DNA polymerase. Libraries were size selected using a
480 3% agarose Pippin prep and final libraries were PCR amplified. Samples were sequenced as
481 either single- or paired-end 50 nt reads on either a NextSeq550 or NovaSeq.
482

483 **Mitoribosome profiling analysis**

484 Adapter sequences were removed with cutadapt and aligned with bowtie2 to a fasta containing
485 rRNA and tRNA sequences. To identify stalling sites, reads were mapped to a custom

486 mitochondrial transcriptome containing all 5' UTRs, coding sequences, and 3' UTRs for all
487 processed mRNAs. Reads were aligned with bowtie2. A 13-nt P-site offset was assigned using
488 Plastid and mapping reads relative to the start codons of *ND4*, *ATP6*, *MT-ND5-dORF.* We
489 determined the relative ribosome density by normalizing the number of reads at each codon by
490 the total number of reads mapping to its respective gene for each sample. Fold change was then
491 calculated by dividing the relative ribosome density in a treated sample by that in an untreated
492 sample, excluding sites that carried less than 0.1% of the total ribosome density of each gene. To
493 identify putative novel translation initiation sites, we mapped our footprints to the entire
494 mitochondrial genome and visually inspected the 3' ends of mitochondrial tRNAs and rRNAs.
495
496 **Mass spectrometry analysis of mitochondrial proteins**
497 Mitochondria were isolated from 2 × 10^7 HEK293 cells using the Mitochondria Isolation Kit for
498 Cultured Cells (Thermo Scientific). Mitochondrial proteins were processed for trypsin/LysC
499 digestion, and the digested peptide mixture was then concentrated and desalted using C18
500 column. Reconstituted desalted peptides in 25 µl of 0.1% formic acid. 12 µl of peptides from each
501 sample was analyzed by a 110 min LC/MS/MS run. The LC/MS/MS analysis of tryptic peptides
502 for each sample was performed sequentially with a blank run between each two sample runs
503 using a Thermo Scientific Orbitrap Exploris 240 Mass Spectrometer and a Thermo Dionex
504 UltiMate 3000 RSLCnano System. Peptides from trypsin digestion were loaded onto a peptide
505 trap cartridge at a flow rate of 5 µL/min. The trapped peptides were eluted onto a reversed-phase
506 Easy-Spray Column PepMap RSLC, C18, 2 µM, 100A, 75 µm × 250 mm (Thermo Scientific) using
507 a linear gradient of acetonitrile (3-36%) in 0.1% formic acid. The elution duration was 60 min at a
508 flow rate of 0.3 µl/min. Eluted peptides from the Easy-Spray column were ionized and sprayed
509 into the mass spectrometer, using a Nano Easy-Spray Ion Source (Thermo) under the following
510 settings: spray voltage, 1.6 kV, Capillary temperature, 275°C. Other settings were empirically
511 determined. Raw data files were searched against the human protein sequences database and
512 the client target protein sequences database using the Proteome Discoverer 2.5 software
513 (Thermo, San Jose, CA) based on the SEQUEST algorithm. Carbamidomethylation (+57.021 Da)
514 of cysteines was set as a fixed modification, and Oxidation / +15.995 Da (M), Phospho / +79.966
515 Da (S, T, Y), and Deamidated / +0.984 Da (N, Q) were set as dynamic modifications. The
516 minimum peptide length was specified to be five amino acids. The precursor mass tolerance was
517 set to 15 ppm, whereas the fragment mass tolerance was set to 0.05 Da. The maximum false
518 peptide discovery rate was specified as 0.01. The resulting Proteome Discoverer Report contains

all assembled proteins with peptides sequences and peptide spectrum match counts (PSM#) and MS1 peak area relative abundance.

Data sharing

Mitoribosome fastq files, wig files mapping to mitochondrial mRNAs, and read length files for MNase-treated samples mapping to chrM are available through GEO Series GSE277563.

Author contributions

J.M. conceived the project, designed and executed experiments, analyzed data, and wrote the manuscript. E.Y. analyzed mitoribosome profiling data. M.H. supervised the project, advised on data interpretation and experimental design, and edited the manuscript.

Acknowledgments

We'd like to thank Nicholas Guydosh (NIDDK), Sezen Meydan (Vanderbilt University), Astrid Haase (NIDDK), the Haase lab members, and the Hafner lab members for their feedback on this work. We thank Daniel Benhalvey (Tel Aviv University) for his assistance in carrying out ribosome profiling and Sarah Young-Baird (Uniformed Services University) for assistance with sucrose gradient fractionation. We thank Stefania Dell'Orso and Faiza Naz (NIH/NIAMS Genomic Technology Section) for sequencing experiments. This research was supported by the Intramural Research Program of the National Institutes of Health (NIH). The contributions of the NIH authors are considered Works of the United States Government. The findings and conclusions presented in this paper are those of the authors and do not necessarily reflect the views of the NIH or the U.S. Department of Health and Human Services.

Funding

Intramural Research Program of the National Institutes of Health, National Institute of Arthritis and Musculoskeletal and Skin Diseases (ZIA-AR041205 to M.H.).

547

548 # Supplementary Figures and Tables

	Nucleotide 1	Nucleotide 2	Nucleotide 3
MT-ND1	0.407	0.321	0.272
MT-ND2	0.381	0.332	0.287
MT-CO1	0.406	0.297	0.297
MT-CO2	0.396	0.314	0.290
MT-ATP8	0.386	0.303	0.311
MT-ATP6	0.382	0.321	0.297
MT-CO3	0.387	0.304	0.308
MT-ND3	0.404	0.302	0.293
MT-ND4L	0.359	0.347	0.294
MT-ND4	0.418	0.302	0.280
MT-ND5	0.385	0.337	0.278
MT-ND6	0.369	0.294	0.338
MT-CYB	0.408	0.304	0.287
MT-RNR1_ORF	0.365	0.347	0.288
MT-RNR1_ncRNA	0.338	0.331	0.331
MT-Humanin	0.345	0.376	0.279
MT-TI	0.030	0.685	0.284
MT-TS1	0.245	0.460	0.296

549

550 **Table S1. Read phasing values for mitoribosomes footprinted with RNaseI.**
551 The read phasing values for the canonical and putative ORFs.
552

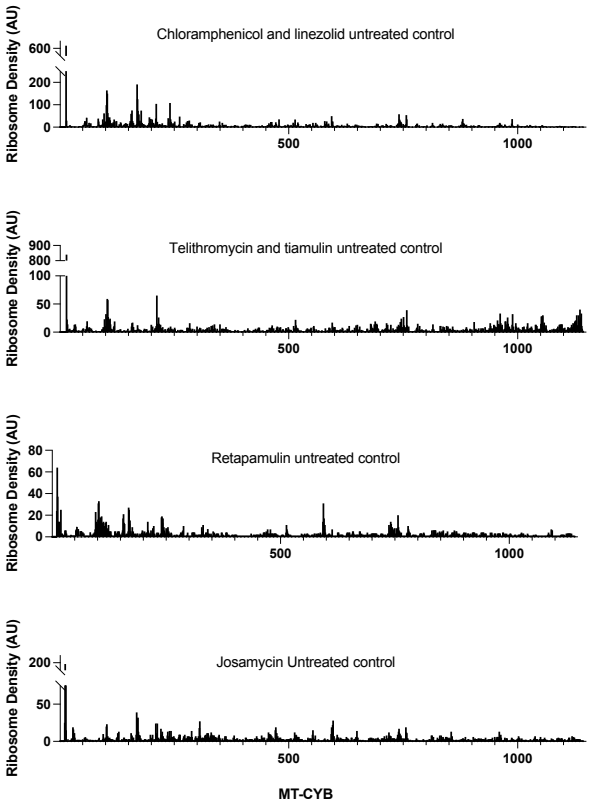

553
554 **Figure S1. Mitoribosome profiling traces of *MT-CYB*.**
555 Individual traces from mitoribosome profiling from each untreated control labeled with its'
556 corresponding antibiotic-treated sample.
557
558
559

A

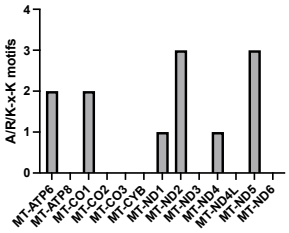

B

Gene	Stall site (codon)	Log Fold Change	Stall Motif	Length of Gene (codons)
MT-ND4	80	55.66929134	RKK	459
MT-ND2	104	34.63291139	AMK	347
MT-ATP6	96	13.34866237	KIK	226
MT-CO1	480	8.44860196	KRK	513
MT-ATP6	94	7.213050223	RSK	226
MT-ND1	53	6.980821918	AMK	318
MT-ND5	511	6.752314298	KLK	603
MT-ND2	57	4.222222222	AIK	347
MT-CO1	478	4.049649208	ASK	513
MT-ND2	313	2.738072055	KMK	347
MT-ND5	513	1.706953542	KMK	603
MT-ND5	222	0.9491412	AGK	603

Figure S2. Distribution of A/R/K-X-K telithromycin stalling site.
(A) The frequency of each telithromycin stalling sites across canonical mtDNA-encoded genes and (B) the measured log fold change at those sites as compared to an untreated control.

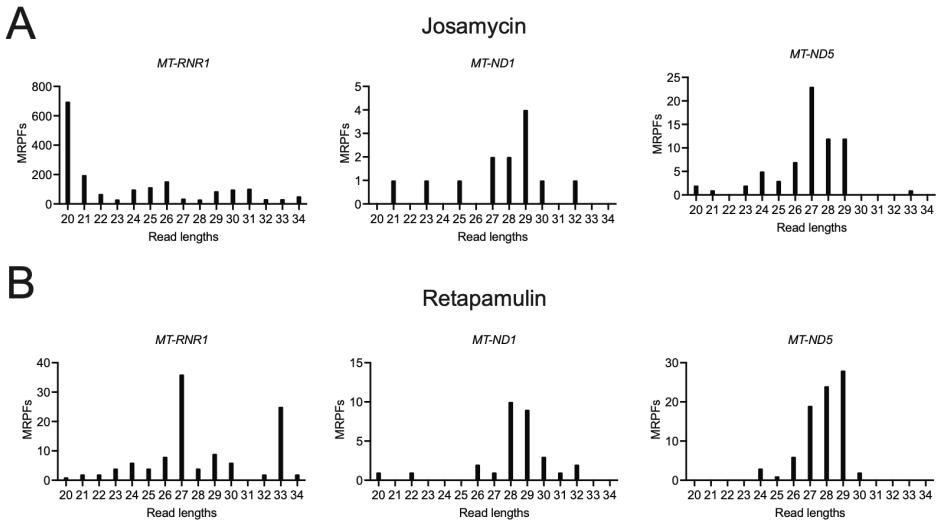

Figure S3. MRPF lengths after treatment with initiation inhibitors correlate to alternative initiation sites.

(A) Read lengths of MNase-generated MRPFs from cells treated with josamycin or (B) retapamulin.

Supplementary Files

Supplemental File 1

Peptides identified by protein mass spectrometry of isolated mitochondria.

References

1. Gray, M.W., Burger, G., and Lang, B.F. (1999). Mitochondrial evolution. Science *283*, 1476-1481. 10.1126/science.283.5407.1476.
2. D'Souza, A.R., and Minczuk, M. (2018). Mitochondrial transcription and translation: overview. Essays Biochem *62*, 309-320. 10.1042/EBC20170102.
3. Enriquez, J.A., Chomyn, A., and Attardi, G. (1995). MtDNA mutation in MERRF syndrome causes defective aminoacylation of tRNA(Lys) and premature translation termination. Nat Genet *10*, 47-55. 10.1038/ng0595-47.
4. Webb, B.D., Diaz, G.A., and Prasun, P. (2020). Mitochondrial translation defects and human disease. J Transl Genet Genom *4*, 71-80. 10.20517/jtgg.2020.11.
5. Prezant, T.R., Agapian, J.V., Bohlman, M.C., Bu, X., Oztas, S., Qiu, W.Q., Arnos, K.S., Cortopassi, G.A., Jaber, L., Rotter, J.I., and et al. (1993). Mitochondrial ribosomal RNA mutation associated with both antibiotic-induced and non-syndromic deafness. Nat Genet *4*, 289-294. 10.1038/ng0793-289.
6. Zheng, J., Ji, Y., and Guan, M.X. (2012). Mitochondrial tRNA mutations associated with deafness. Mitochondrion *12*, 406-413. 10.1016/j.mito.2012.04.001.
7. Smick, K.M., Condit, P.K., Proctor, R.L., and Sutcher, V. (1964). Fatal Aplastic Anemia. An Epidemiological Study of Its Relationship to the Drug Chloramphenicol. J Chronic Dis *17*, 899-914. 10.1016/0021-9681(64)90161-4.
8. Woodhead, J.L., Yang, K., Oldach, D., MacLauchlin, C., Fernandes, P., Watkins, P.B., Siler, S.Q., and Howell, B.A. (2019). Analyzing the Mechanisms Behind Macrolide Antibiotic-Induced Liver Injury Using Quantitative Systems Toxicology Modeling. Pharm Res *36*, 48. 10.1007/s11095-019-2582-y.
9. De Vriese, A.S., Coster, R.V., Smet, J., Seneca, S., Lovering, A., Van Haute, L.L., Vanopdenbosch, L.J., Martin, J.J., Groote, C.C., Vandecasteele, S., and Boelaert, J.R. (2006). Linezolid-induced inhibition of mitochondrial protein synthesis. Clin Infect Dis *42*, 1111-1117. 10.1086/501356.
10. Gupta, A., Okesli-Armlovich, A., Morgens, D., Bassik, M.C., and Khosla, C. (2020). A genome-wide analysis of targets of macrolide antibiotics in mammalian cells. J Biol Chem *295*, 2057-2067. 10.1074/jbc.RA119.010770.
11. Amunts, A., Brown, A., Toots, J., Scheres, S.H.W., and Ramakrishnan, V. (2015). Ribosome. The structure of the human mitochondrial ribosome. Science *348*, 95-98. 10.1126/science.aaa1193.
12. Fu, X., Wan, P., Li, P., Wang, J., Guo, S., Zhang, Y., An, Y., Ye, C., Liu, Z., Gao, J., et al. (2021). Mechanism and Prevention of Ototoxicity Induced by Aminoglycosides. Front Cell Neurosci *15*, 692762. 10.3389/fncel.2021.692762.
13. Morales-Alvarez, M.C. (2020). Nephrotoxicity of Antimicrobials and Antibiotics. Adv Chronic Kidney Dis *27*, 31-37. 10.1053/j.ackd.2019.08.001.
14. Soriano, A., Miro, O., and Mensa, J. (2005). Mitochondrial toxicity associated with linezolid. N Engl J Med *353*, 2305-2306. 10.1056/NEJM200511243532123.
15. Palenzuela, L., Hahn, N.M., Nelson, R.P., Jr., Arno, J.N., Schobert, C., Bethel, R., Ostrowski, L.A., Sharma, M.R., Datta, P.P., Agrawal, R.K., et al. (2005). Does linezolid cause lactic acidosis by inhibiting mitochondrial protein synthesis? Clin Infect Dis *40*, e113-116. 10.1086/430441.
16. Bale, B.I., Elebesunu, E.E., Manikavasagar, P., Agwuna, F.O., Ogunkola, I.O., Sow, A.U., and Lucero-Prisno, D.E., 3rd (2023). Antibiotic resistance in ocular bacterial infections: an

626 integrative review of ophthalmic chloramphenicol. Trop Med Health *51*, 15.
627 10.1186/s41182-023-00496-x.
628 17. Lorenzo, D. (2019). Chloramphenicol Resurrected: A Journey from Antibiotic Resistance
629 in Eye Infections to Biofilm and Ocular Microbiota. Microorganisms *7*.
630 10.3390/microorganisms7090278.
631 18. Browne, A.J., Chipeta, M.G., Haines-Woodhouse, G., Kumaran, E.P.A., Hamadani,
632 B.H.K., Zaraa, S., Henry, N.J., Deshpande, A., Reiner, R.C., Jr., Day, N.P.J., et al. (2021).
633 Global antibiotic consumption and usage in humans, 2000-18: a spatial modelling study.
634 Lancet Planet Health *5*, e893-e904. 10.1016/S2542-5196(21)00280-1.
635 19. Graham, D.J. (2006). Telithromycin and acute liver failure. N Engl J Med *355*, 2260-2261.
636 10.1056/NEJMc066372.
637 20. Paternoga, H., Crowe-McAuliffe, C., Bock, L.V., Koller, T.O., Morici, M., Beckert, B.,
638 Myasnikov, A.G., Grubmuller, H., Novacek, J., and Wilson, D.N. (2023). Structural
639 conservation of antibiotic interaction with ribosomes. Nat Struct Mol Biol *30*, 1380-1392.
640 10.1038/s41594-023-01047-y.
641 21. Lin, J., Zhou, D., Steitz, T.A., Polikanov, Y.S., and Gagnon, M.G. (2018). Ribosome-
642 Targeting Antibiotics: Modes of Action, Mechanisms of Resistance, and Implications for
643 Drug Design. Annu Rev Biochem *87*, 451-478. 10.1146/annurev-biochem-062917-
644 011942.
645 22. Yan, K., Madden, L., Choudhry, A.E., Voigt, C.S., Copeland, R.A., and Gontarek, R.R.
646 (2006). Biochemical characterization of the interactions of the novel pleuromutilin
647 derivative retapamulin with bacterial ribosomes. Antimicrob Agents Chemother *50*, 3875-
648 3881. 10.1128/AAC.00184-06.
649 23. Meydan, S., Marks, J., Klepacki, D., Sharma, V., Baranov, P.V., Firth, A.E., Margus, T.,
650 Kefi, A., Vazquez-Laslop, N., and Mankin, A.S. (2019). Retapamulin-Assisted Ribosome
651 Profiling Reveals the Alternative Bacterial Proteome. Mol Cell *74*, 481-493 e486.
652 10.1016/j.molcel.2019.02.017.
653 24. Choi, J., Marks, J., Zhang, J., Chen, D.H., Wang, J., Vazquez-Laslop, N., Mankin, A.S.,
654 and Puglisi, J.D. (2020). Dynamics of the context-specific translation arrest by
655 chloramphenicol and linezolid. Nat Chem Biol *16*, 310-317. 10.1038/s41589-019-0423-2.
656 25. Marks, J., Kannan, K., Roncase, E.J., Klepacki, D., Kefi, A., Orelle, C., Vazquez-Laslop,
657 N., and Mankin, A.S. (2016). Context-specific inhibition of translation by ribosomal
658 antibiotics targeting the peptidyl transferase center. Proc Natl Acad Sci U S A *113*, 12150-
659 12155. 10.1073/pnas.1613055113.
660 26. Itoh, Y., Singh, V., Khawaja, A., Naschberger, A., Nguyen, M.D., Rorbach, J., and Amunts,
661 A. (2022). Structure of the mitoribosomal small subunit with streptomycin reveals Fe-S
662 clusters and physiological molecules. Elife *11*. 10.7554/eLife.77460.
663 27. Amunts, A., Brown, A., Bai, X.C., Llacer, J.L., Hussain, T., Emsley, P., Long, F.,
664 Murshudov, G., Scheres, S.H.W., and Ramakrishnan, V. (2014). Structure of the yeast
665 mitochondrial large ribosomal subunit. Science *343*, 1485-1489.
666 10.1126/science.1249410.
667 28. Li, S.H., Nofal, M., Parsons, L.R., Rabinowitz, J.D., and Gitai, Z. (2021). Monitoring
668 mammalian mitochondrial translation with MitoRiboSeq. Nat Protoc *16*, 2802-2825.
669 10.1038/s41596-021-00517-1.
670 29. Rooijers, K., Loayza-Puch, F., Nijtmans, L.G., and Agami, R. (2013). Ribosome profiling
671 reveals features of normal and disease-associated mitochondrial translation. Nat
672 Commun *4*, 2886. 10.1038/ncomms3886.
673 30. Sothiselvam, S., Neuner, S., Rigger, L., Klepacki, D., Micura, R., Vazquez-Laslop, N., and
674 Mankin, A.S. (2016). Binding of Macrolide Antibiotics Leads to Ribosomal Selection

against Specific Substrates Based on Their Charge and Size. Cell Rep *16*, 1789-1799. 10.1016/j.celrep.2016.07.018.

31. Schlunzen, F., Pyetan, E., Fucini, P., Yonath, A., and Harms, J.M. (2004). Inhibition of peptide bond formation by pleuromutilins: the structure of the 50S ribosomal subunit from Deinococcus radiodurans in complex with tiamulin. Mol Microbiol *54*, 1287-1294. 10.1111/j.1365-2958.2004.04346.x.

32. Poulsen, S.M., Karlsson, M., Johansson, L.B., and Vester, B. (2001). The pleuromutilin drugs tiamulin and valnemulin bind to the RNA at the peptidyl transferase centre on the ribosome. Mol Microbiol *41*, 1091-1099. 10.1046/j.1365-2958.2001.02595.x.

33. Davidovich, C., Bashan, A., Auerbach-Nevo, T., Yaggie, R.D., Gontarek, R.R., and Yonath, A. (2007). Induced-fit tightens pleuromutilins binding to ribosomes and remote interactions enable their selectivity. Proc Natl Acad Sci U S A *104*, 4291-4296. 10.1073/pnas.0700041104.

34. Arenz, S., Ramu, H., Gupta, P., Berninghausen, O., Beckmann, R., Vazquez-Laslop, N., Mankin, A.S., and Wilson, D.N. (2014). Molecular basis for erythromycin-dependent ribosome stalling during translation of the ErmBL leader peptide. Nat Commun *5*, 3501. 10.1038/ncomms4501.

35. Beckert, B., Leroy, E.C., Sothiselvam, S., Bock, L.V., Svetlov, M.S., Graf, M., Arenz, S., Abdelshahid, M., Seip, B., Grubmuller, H., et al. (2021). Structural and mechanistic basis for translation inhibition by macrolide and ketolide antibiotics. Nat Commun *12*, 4466. 10.1038/s41467-021-24674-9.

36. Dubot, A., Godinot, C., Dumur, V., Sablonniere, B., Stojkovic, T., Cuisset, J.M., Vojtiskova, A., Pecina, P., Jesina, P., and Houstek, J. (2004). GUG is an efficient initiation codon to translate the human mitochondrial ATP6 gene. Biochem Biophys Res Commun *313*, 687-693. 10.1016/j.bbrc.2003.12.013.

37. Kruger, A., Remes, C., Shiriaev, D.I., Liu, Y., Spahr, H., Wibom, R., Atanassov, I., Nguyen, M.D., Cooperman, B.S., and Rorbach, J. (2023). Human mitochondria require mtRF1 for translation termination at non-canonical stop codons. Nat Commun *14*, 30. 10.1038/s41467-022-35684-6.

38. Tsai, K., Stojkovic, V., Lee, D.J., Young, I.D., Szal, T., Klepacki, D., Vazquez-Laslop, N., Mankin, A.S., Fraser, J.S., and Fujimori, D.G. (2022). Structural basis for context-specific inhibition of translation by oxazolidinone antibiotics. Nat Struct Mol Biol *29*, 162-171. 10.1038/s41594-022-00723-9.

39. Syroegin, E.A., Flemmich, L., Klepacki, D., Vazquez-Laslop, N., Micura, R., and Polikanov, Y.S. (2022). Structural basis for the context-specific action of the classic peptidyl transferase inhibitor chloramphenicol. Nat Struct Mol Biol *29*, 152-161. 10.1038/s41594-022-00720-y.

40. Wakigawa, T., Mito, M., Yamashiro, H., Tomuro, K., Tani, H., Tomizawa, K., Chujo, T., Nagao, A., Suzuki, T., Wei, F.-Y., et al. (2023). Complexity and dynamics of in organello translation landscape assessed by high-resolution mitochondrial ribosome profiling. bioRxiv, 2023.2007.2019.549812. 10.1101/2023.07.19.549812.

41. Bibel, B., Raskar, T., Couvillion, M., Lee, M., Kleinman, J.I., Takeuchi-Tomita, N., Churchman, L.S., Fraser, J.S., and Fujimori, D.G. (2024). Context-specific inhibition of mitochondrial ribosomes by phenicol and oxazolidinone antibiotics. bioRxiv, 2024.2008.2021.609012. 10.1101/2024.08.21.609012.

42. Brandon, M.C., Lott, M.T., Nguyen, K.C., Spolim, S., Navathe, S.B., Baldi, P., and Wallace, D.C. (2005). MITOMAP: a human mitochondrial genome database--2004 update. Nucleic Acids Res *33*, D611-613. 10.1093/nar/gki079.

43. Kalghatgi, S., Spina, C.S., Costello, J.C., Liesa, M., Morones-Ramirez, J.R., Slomovic, S., Molina, A., Shirihai, O.S., and Collins, J.J. (2013). Bactericidal antibiotics induce

725 mitochondrial dysfunction and oxidative damage in Mammalian cells. Sci Transl Med *5*,
726 192ra185. 10.1126/scitranslmed.3006055.
727 44. D'Achille, G., and Morroni, G. (2023). Side effects of antibiotics and perturbations of
728 mitochondria functions. Int Rev Cell Mol Biol *377*, 121-139.
729 10.1016/bs.ircmb.2023.03.009.
730 45. Desai, N., Yang, H., Chandrasekaran, V., Kazi, R., Minczuk, M., and Ramakrishnan, V.
731 (2020). Elongational stalling activates mitoribosome-associated quality control. Science
732 *370*, 1105-1110. 10.1126/science.abc7782.
733 46. Singh, V., Itoh, Y., Del'Olio, S., Hassan, A., Naschberger, A., Flygaard, R.K., Nobe, Y.,
734 Izumikawa, K., Aibara, S., Andrell, J., et al. (2024). Mitoribosome structure with cofactors
735 and modifications reveals mechanism of ligand binding and interactions with L1 stalk. Nat
736 Commun *15*, 4272. 10.1038/s41467-024-48163-x.
737 47. Kong, Q.P., Yao, Y.G., Sun, C., Zhu, C.L., Zhong, L., Wang, C.Y., Cai, W.W., Xu, X.M.,
738 Xu, A.L., and Zhang, Y.P. (2004). Phylogeographic analysis of mitochondrial DNA
739 haplogroup F2 in China reveals T12338C in the initiation codon of the ND5 gene not to be
740 pathogenic. J Hum Genet *49*, 414-423. 10.1007/s10038-004-0170-3.
741 48. Vilarinho, L., Chorao, R., Cardoso, M.L., Rocha, H., Nogueira, C., and Santorelli, F.M.
742 (1999). The ND1 T3308C mutation may be a mtDNA polymorphism. Report of two
743 Portuguese patients. J Inherit Metab Dis *22*, 90-91. 10.1023/a:1005471904710.
744 49. Rocha, H., Flores, C., Campos, Y., Arenas, J., Vilarinho, L., Santorelli, F.M., and Torroni,
745 A. (1999). About the "Pathological" role of the mtDNA T3308C mutationellipsis. Am J Hum
746 Genet *65*, 1457-1459. 10.1086/302641.
747 50. Soto, I., Couvillion, M., Hansen, K.G., McShane, E., Moran, J.C., Barrientos, A., and
748 Churchman, L.S. (2022). Balanced mitochondrial and cytosolic translatomes underlie the
749 biogenesis of human respiratory complexes. Genome Biol *23*, 170. 10.1186/s13059-022-
750 02732-9.
751 51. Fiedler, M., Rossmanith, W., Wahle, E., and Rammelt, C. (2015). Mitochondrial poly(A)
752 polymerase is involved in tRNA repair. Nucleic Acids Res *43*, 9937-9949.
753 10.1093/nar/gkv891.
754